MISS JINDAPORN JUTHAPAKDEEPRASERT (Orcid ID : 0000-0003-0520-8129)

MR. WIRAT LERDPROM (Orcid ID : 0000-0001-6483-802X)

Article type : Article

Corresponding author mail id: jj1916@ic.ac.uk

Reactions and emissivity of cerium oxide with phosphate binder coating on basic refractory brick

Jindaporn Juthapakdeeprasert[1], Oriol Gavalda Diaz[1], Wirat Lerdprom[1], Domingos De Sousa Meneses[2], Doni D. Jayaseelan[3] and William E Lee [1]

[1] Centre for Advanced Structural Ceramics (CASC), Department of Materials, Imperial College London, South Kensington Campus, London, SW7 2AZ, United Kingdom

[2] CNRS, CEMHTI UPR3079, University Orléans, F-45071 Orléans, France

[3] Department of Aerospace and Aircraft Engineering, Kingston University London, Roehampton Vale Campus, London, SW15 3DW, United Kingdom

Abstract

High emissivity coatings which aim to help the cement industry reduce heat loss in its production process have been developed with different CeO_2 and $AlH_6O_{12}P_3$ ratios (1:3, 1:5 and 1:12 by volume). The coating slurries were shear thinning and after heat treatment in air at 1300°C, 1°C/min, dwell 3 hr, XRD revealed that $CePO_4$ forms more easily as the Ce/P ratio decreases. The composition with a 1:5 ratio of CeO_2:$AlH_6O_{12}P_3$ was gun sprayed on basic refractory bricks, then heat treated under the same conditions as the slurries. SEM, (S)TEM and EDX were used to study thickness, microstructure and chemical

This article has been accepted for publication and undergone full peer review but has not been through the copyediting, typesetting, pagination and proofreading process, which may lead to differences between this version and the Version of Record. Please cite this article as doi: 10.1111/IJAC.13416

composition of the coatings which revealed that the coating was composed of pores, CeO_2 grains, $CePO_4$ grains and M-P-O glass. SEM images show that $CePO_4$ was nucleated from a reaction between CeO_2 and $AlH_6O_{12}P_3$. Consequently, $CePO_4$ grains (~2 μm diameter) were smaller than CeO_2 (~10μm diameter). The emissivities of un-coated and coated basic refractory bricks were measured at 1100 and 1300°C over the wave number range of 700-12000 cm^{-1}. At both temperatures, the emissivity of the coated bricks was higher than the uncoated bricks and the emissivity was measured to be higher at a higher temperature for both samples. The coated bricks gave the highest emissivity of 0.81 from 1050-11000 cm^{-1} which is about twice the un-coated bricks for the same conditions. This demonstrates that the developed high emissivity coating has potential to be used with basic refractory brick.

Introduction

Energy intensive (high temperature) industries face a challenge to enhance energy efficiency and retain as much heat in process as possible. The cement industry is a major energy consumer and cement production uses 3.4GJ/ ton clinker, and the global production is now over 2 billion metric tons annually[1, 2]. Most energy consumption in the cement industry is from heating raw materials to 1450°C in a kiln to achieve required phases; $3CaO{\cdot}SiO_2$, $2CaO{\cdot}SiO_2$, $3CaO{\cdot}Al_2O_3$ and $4CaO{\cdot}Al_2O_3{\cdot}Fe_2O_3$. To make the production more efficient, kilns are continually heated to avoid shutdown cycles where most heat energy is consumed. However, maintaining the kiln at 1450°C requires high amounts of energy due to the temperature difference between inside and outside (environment) of the kiln causing heat loss. This problem can be lowered by reducing heat transfer between the kiln contents and liner materials.

Attempts have been made to reduce the thermal conductivity of refractory bricks used in the cement kiln by using lightweight, porous and foamed materials[3-5]. However, the addition of these materials lowers the strength of the refractory bricks and could lead to operational failure. Also, changing the refractory lining in cement kilns is not an ideal solution because it is a high cost process and requires significant down time. Thermal convection is dependent on the velocity of the fluid (gas or liquid) that carries away the heat which is difficult to setup and control in a large-scale manufacturing process like cement production. Thermal radiation is the most interesting among the heat transfer mechanisms because it is highly dependent on temperature difference (to the 4th power as in Equation 1) making it a more dominant heat transfer mechanism than thermal conduction and convection especially at high temperature[6].

$$Q_{rad} = A\varepsilon\sigma(T_w^4 - T_o^4) \qquad \text{Equation 1}$$

where Q_{rad} is heat in Watts (W)

A is area of heat transfer surface (m^2)

ε is surface emissivity

σ is the Stefan-Boltzmann constant (5.67 x 10^{-8} W/m^2K^4)

T_w is surface temperature (K)

T_o is ambient temperature (K)

Equation 1 reveals that thermal radiative heat transfer is dependent only on the area of the heat transfer surface and not the whole volume, therefore, only the surface of the refractory bricks needs to be treated. Developing a highly radiative coating means the original refractory bricks can still be used. However, coatings are not appropriate for every zone of the cement rotary kiln. The coating zone, where there is the highest temperature (~1450°C) has a partial melt clicker coating on the refractory lining making it an inappropriate zone. The upper transition zone is the zone that has the second-highest temperature (~1300°C) but not high enough to form clinker coating making it a suitable zone for a radiative coating. Therefore, application of highly radiative coatings is aviable approach for cement industry energy saving.

The high radiative coating functions by absorbing thermal energy then radiating it back into the process and reduce the heat transferring to the external environment. Emissivity plays an important role when aiming to develop highly thermal radiative coatings because it is the only factor in Equation 1 that is a material property. Therefore, materials with high emissivity such as rare earth containing compounds, are frequently used as radiative coatings or as thermal barriers for high temperature applications in spacecraft and gas turbines[7-9]. Rare earth materials can be used as pure materials or added as dopants to others materials such as zirconia, zirconium silicate, alumina, aluminium silicates, silica and ZrB_2/SiC to improve their emissivity properties[7, 8, 10, 11]. Cerium oxide (CeO_2) is the most common rare earth material used due to its high melting point (2477°C), high emissivity (0.9 from 1000-2000°C), good base and acid chemical resistance properties and relatively low cost. However, CeO_2 has been widely used for high temperature coatings on nickel-based alloy substrates but not basic refractory bricks[7-9]. This study attempted to understand if it is possible to use CeO_2 as a coating raw material on a basic refractory that can emit heat. To do so, a binder must also be used to enable application and attachment of CeO_2 onto the substrate. Phosphate binder is a known binder that can resist high temperature and therefore was chosen for this study[4, 12, 13].

Experimental procedure

The substrate used in this work is a basic refractory; BR (80wt% MgO and 20wt% $MgAl_2O_4$), supplied by The Siam Refractory Industry Co., Ltd, Saraburi, Thailand. The coating slurry was prepared by mixing CeO_2 with average particle size of 10 μm (cerium (IV) oxide, 99.5%, Alfa Aesar, Lancashire, England) with $AlH_6O_{12}P_3$ binder (50 wt% aqueous solution, Alfa Aesar, Lancashire, England) in the ratios 1:3, 1:5 and 1:12 by volume using a magnetic stirrer for 2h. The coatings were characterised in both slurry (rheology) and solid (phase analysis, microstructure and emissivity) form.

Rheology of three different compositions was measured using a hybrid rheometer, (Discovery HR-1, TA Instruments, Delaware, USA). Rheology was determined by measuring the viscosity of the slurry with shear rates ranging from 1-100s^{-1} at 25°C within 60 seconds. Three measurements were made for each composition and the curves were used to understand the viscosity of the three coatings.

Phase analysis was carried out for the three coating compositions. After mixing, the coating slurries were heat treated with heating rate of 10°C/min to 1300°C with 3 h dwell. The coatings were then ground in a mortar with a pestle to powder <150μm. The powder was then analysed by X-ray diffraction (XRD, D2 phaser, Bruker, Germany) using Cu-Kα radiation of wavelength, 1.54 Å over 25-60° 2θ with count time of 1 second and step size of 0.034°. The peaks were identified with powder diffraction file standards from the International Centre for Diffraction (ICDD); PDF-4+ card 00-034-0394 for CeO_2 and 00-032-0199 for $CePO_4$.

The coating with 1:5 ratio of CeO_2:$AlH_6O_{12}P_3$ was selected for the microstructure analysis and emissivity measurements. The ratio of 1:5 was chosen because it was fluid enough to be sprayable (1:12 was not sufficiently viscous) and contained enough CeO_2 content to make the principle cost of the coating reasonable. 1:3 has sprayable viscosity but has higher CeO_2 content than 1:5 and therefore the principle cost is higher. The coating was prepared by the same procedure as for the rheology study. After mixing, the slurry was gun sprayed (coated) onto the BR. The coated BR (CBR) samples were dried overnight at room temperature, and then heat treated with a heating rate of 1°C/min for 3h at 1300°C. The thickness and microstructure of the coating cross section was analysed using scanning electron microscopy (SEM, Zeiss Leo Gemini 1525, Oberkochen, Germany) at an accelerating voltage of 5-20 kV using secondary electron imaging. Semi-quantitative area chemical analysis was performed using energy-dispersive spectroscopy (EDX, X-MaX20, Oxford Instruments, Abingdon, UK). The average atomic percentages of each phase were measured in three different areas.

CBR 1:5 microstructure was further studied via TEM/STEM JEM-2100F (JEOL, Japanese Electron Optics Limited, Japan) equipped with an EDX X-Max detector (Oxford Instruments, Abingdon, UK). The sample was imaged at an accelerating voltage of 200 kV. Electron transparent samples were prepared following a standard FIB (Focussed Ion Beam) lift-out technique with a DualBeam Helios NanoLab SEM (FEI, Field Electron and Ion Company, USA), from cross sections of the coating which was applied on the substrate and heat treated as for the samples prepared for the SEM.

The heat transfer performance of coatings was defined by emissivity. Emissivity measurements were carried out at CNRS-CEMHTI[14]. The emissivity apparatus consisted of two Bruker spectrometers; Vertex 80V and Vertex 70 (Germany). Vertex 80V was used for measuring emissivity in the 700-4000 cm^{-1} range (mid-IR) with DLaTGS/KBr detector. Vertex 70 was used to measured two ranges; 4000-9000 cm^{-1} (near-IR) with InGaAs detector and 9000-12000 cm^{-1} (near-IR) with Si-diode detector. After measuring the emissivity of the three wavenumber ranges, data were merged creating emissivity data ranging from 700-12000 cm^{-1} (mid-IR to near-IR). For each individual measurement over each wavenumber range, three sub-measurements were carried out; flux measurement of the sample, blackbody furnace and ambient contribution. Flux of the sample and blackbody furnace were needed to calculate the emissivity referring to the definition which is flux emitted from the sample surface over flux emitted by a blackbody at the same temperature. Ambient (background) contribution was determined so the effect of the instrument surrounding could be removed giving a more accurate emissivity measurement.

BR and CBR, were heated with a CO_2 laser and their emissivity was measured at 1100 and 1300°C. The CO_2 laser power determines the sample temperature. Five powers were used in this experiment, to achieve temperatures shown in Table 1. From Table 1, power of 54 and 71 watts gave the closest temperature to 1100 and 1300°C, respectively for BR and power of 71 and 100 watts gave the closest temperature to 1100 and 1300°C, respectively for CBR. The BR and CBR used different power to reach the same temperature because material with higher heat absorption required higher power to reach desired temperature. With an average of 20°C fluctuation of the instrument shown in previous study, these power levels were chosen for emissivity analysis[14].

Results and Discussion

Coating viscosities (Pa.s) at different shear rates (1/s) on a log scale are shown in Figure 1. The slurry with the ratio of 1:3 has the highest viscosity followed by 1:5 and 1:12. This is attributed to the solid (CeO_2 powder) content. All three coating compositions reveal a shear thinning effect; viscosity decreases as the

shear rate increases. Shear thinning is a pre-requisite for the surface coatings. This is because the coating is applied onto the substrate via gun air spraying where low viscosity is required when pressure (high shear rate) is applied to push the coating through the nozzle. When the slurry is coated on the substrate (low shear rate) it is required to have a high viscosity so that it does not slip off. This is shown schematically in Figure 2.

Phases of the three coatings containing different volume ratios of CeO_2:$AlH_6O_{12}P_3$ (1:3, 1:5 and 1:12) were analysed by XRD (Figure 3) revealing different phases present in the coatings. Figure 3a reveals that all three coatings contain CeO_2 and $CePO_4$. CeO_2 is from the raw material and $CePO_4$ is from the reaction between CeO_2 and $AlH_6O_{12}P_3$[15]. Mixing different CeO_2: $AlH_6O_{12}P_3$ ratios consequently gives rise to different amounts of $CePO_4$ phase and unreacted CeO_2 as indicated by different peak intensities/area. As expected, the 1:3 ratio CeO_2: $AlH_6O_{12}P_3$ has the highest CeO_2 content, therefore, after heat treating, it has the highest CeO_2 and the lowest $CePO_4$ peak intensities. CeO_2 peak intensity decreases and $CePO_4$ peak intensity increases as the CeO_2: $AlH_6O_{12}P_3$ ratio decreases. This can be seen clearly in Figure 3b which is a magnified image of Figure 3a (2theta ranging from 25-35^o) where the highest peaks of both CeO_2 and $CePO_4$ are presented.

The formation of $CePO_4$ from CeO_2 and $AlH_6O_{12}P_3$ is consistent with previous studies. Tsuhaka et al. [13] prepared rare earth phosphate in various ways. One was mixing cerium oxide (CeO_2) with phosphoric acid (H_3PO_4) in Ce/P ratios (R) from 1-50 and heat treating for 20 h at 800^{o}C. They reported that most $CePO_4$ forms when R = 1-2. At higher Ce/P atomic ratios other phases also form such as CeP_2O_7 $Ce(PO_3)_3$ and $Ce(PO_3)_4$. This means that the lower the Ce/P ratio the more $CePO_4$ can be formed [16]. In this experiment, the ratios of CeO_2 to $AlH_6O_{12}P_3$ were 1:3, 1:5 and 1:12 vol ratios which are 2.5, 1.2 and 0.5 Ce/P atomic ratios respectively. The 1:5 vol ratios (1.2 Ce/P atomic ratios) fall into the R=1-2 range and therefore show higher XRD intensity of $CePO_4$ than in the 1:3 ratios (2.5 atomic ratios). This trend is similar to that reported by Tsuhaka et al [13] i.e. the lower the amount of CeO_2 in the system, the easier $CePO_4$ can be formed.

The microstructure of the 1:5-CeO_2:$AlH_6O_{12}P_3$ cross section was analysed using SEM. Examination of the coating (Figure 4a) clearly distinguished the coating and substrate. Coating thickness was 290 $\pm$15 μm measured from Figure 4a. The coating contained 4 features; pores, large grains (~10μm), small grains (~2μm) and a phase with a smoothed morphology indicative of melting (matrix). The 4 features are shown in Figure 4b. Pores are generated from dehydrogenation of $AlH_6O_{12}P_3$ as temperature increases [13, 17]. The large and small grains were identified by EDX analysis as CeO_2 and $CePO_4$ respectively (Figure 4c). $CePO_4$

formed by a nucleation mechanism and therefore the grains are much smaller than CeO_2. The matrix is mostly composed of magnesium (Mg), phosphorus (P) and oxygen (O), also revealed by EDX. Magnesium is from the substrate, phosphorus from the binder and oxygen from both. The atomic ratio of the Mg-P-O is close to 1:1:4 and therefore, it is likely that this matrix is magnesium phosphate ($MgPO_4$). EDX mapping in Figure 5 confirms that there was no obvious reaction between the substrate (MgO and $MgO{\cdot}Al_2O_3$ spinel) and the coating (CeO_2, $CePO_4$ and matrix). There was only slight MgO migration from the substrate into the coating and of P from the coating into the substrate.

The microstructures revealed by this experiment combined with previous studies[12] on interactions between CeO_2 and $AlH_6O_{12}P_3$ make it possible to produce a schematic (Figure 6) of how the coating changes as temperature increases. At room temperature, the coating contained two materials which are CeO_2 and $AlH_6O_{12}P_3$ in the ratio of 1:5 vol. When the coating was left to dry, CeO_2 particles sediment. When heat is given to the system and increases the temperature, dehydrogenation of $AlH_6O_{12}P_3$ occurs generating pores. Pores rising to the surface of the coating bringing along some of the CeO_2 and $CePO_4$ particles with them. As temperature continues to increase, $CePO_4$ forms [15, 16]. At the same time, remaining CeO_2 particles sinter. To achieve a more homogeneous coating, a dispersion can be added to avoid sedimentation of CeO_2. However, due to the large particle size (~10μm) of the CeO_2, which was used as commercially received, and high density (heavy), the CeO_2 powder might need to be subject to further grinding.

Transformation of CeO_2 to $CePO_4$ influences the coatings light emission behaviour in the visible range (12500-25000 cm^{-1}) because CeO_2 contains Ce^{4+} while $CePO_4$ contains Ce^{3+}. The significant difference between the 2 valence states of Ce is that the Ce 4f orbital in the Ce^{4+} electronic structure participates in the chemical bonding of CeO_2 and partially loses its f-character so it does not have a valence band close to the Fermi edge (<2.5eV difference). Having a valence band close to the Fermi edge can benefit emissivity in the visible range because lower energy; possibly as low as 2.5eV, is needed for the electrons to be absorbed and become excited before the energy is re-emitted[18, 19]. However, this study is more concerned with heat emission which is in the infrared range and CeO_2 and $CePO_4$ would be expected to give similar emissivity in this range because infrared electromagnetic wave energy is only high enough to vibrate/rotate the bonds and not to excite electrons from valence band to a excited state.

Further study on the microstructure was done with (S)TEM and EDX. The area selected for the characterization contained the small particles and matrix as shown in Figure 7a. EDX was used to conduct element mapping to understand the chemical composition, Figure 7b, revealing that the particles contained Ce-P-O and the matrix contained M-P-O. Matching the EDX mapping with the XRD analysis

indicates that the particles are $CePO_4$. As confirmed by electron diffraction (Figure 7c). The d-spacings and plane angles were measured and compared with the $CePO_4$ electron diffraction pattern reference revealing a match with $CePO_4$ monoclinic single crystal structure down the [001] zone axis. As for the matrix, Figure 7d, the likely melted phase did not show any diffraction spots confirming it has a glassy structure. Therefore, the likely melted phase is magnesium phosphate glass.

Emissivity results of BR and CBR samples measured at 1100 and 1300oC are shown in Figure 8. Figure 8a reveals emissivity of BR at 1100, 1300^{o}C and CBR at 1100^{o}C decreases in the wavenumber range of 1000-3000 cm^{-1}. This is a trend commonly observed for dielectric materials. However, as the wavenumber continues to increase, the emissivity starts to increase. As Kirchhoff's law implies that the microscopic mechanisms producing thermal emission are also responsible for absorption at the same wavelengths, explaining emission can be made by a discussion of the origin of absorption. In general, absorption is separated into 3 mechanisms; interband absorption, free-carrier absorption and lattice absorption. Interband absorption is when electrons are excited over an interband (move from a valence band to another band). Interband absorption mostly occurs in the short wavelength range (visible-ultraviolet) due to it requires the energy to excite the electrons over a wide bandgap. Free-carrier absorption is electrons/holes excited by absorbing a photon and move over an intraband (mover from a filled state to an empty state but in the same band). It occurs in metals and semiconductors. Lattice absorption comes from the atomic vibrations (phonons in crystals, typically below 1500 cm^{-1}). In ceria, the strong decrease of emissivity in the wavenumber range of 1000-3000 cm^{-1} is due to the nearly exponential decrease of the absorption coefficient induced by multi-phonon processes (20). The progressive increase of emissivity at higher wavenumbers is typical of the response of charge carriers that are not completely free (electronic or hole defects). Their hoping motions are coupled to lattice vibrations (like polaronic absorption). In the case of small polarons, the spectral dependence of the contribution of the hoping motions to the absorption is similar to that observed in Figure 8 and is given by a Debye model. So, for this kind of dielectric materials, the total emissivity is from the charge-carrier absorption and lattice absorption. The emissivity becomes steady from 7000-11000 cm^{-1}. CBR shows a different emissivity spectrum. Its emissivity becomes steady at 0.81 from 3000-12000 cm^{-1}. Figure 8b is a magnified image from a section in Figure 8a revealing that the Christiansen points of the BR and CBR are in the 800-1000 cm^{-1} range. Christiansen points appear at the wavenumber corresponding to the highest emissivity level. They occur when a material's specific frequency for which the refractive index is nearly equal to 1 and its absorption coefficient has a moderate value. These two characteristics explain the very high absorption efficiency of the material and that the compound emits like a blackbody[21]. Other than the Christiansen point, Figure 8b

also revealed two other events. First, a dip of emissivity in the wavenumber range of 950-1050 cm^{-1} due to stretching motions of PO_4 tetrahedra. Second, a sharp dip at 1870-1900cm^{-1} which was a measurement artefact from the CO_2 laser. Comparing the emissivity between BR and CBR shows that the coating improves the emissivity of BR especially at 1300°C by 120% (Figure 8). As the temperature increase, there is an activation of charge hoping in the CeO_2/$CePO_4$ applied coating which leads to higher absorption/emission. This suggests that CeO_2 and $AlH_6O_{12}P_3$ can provide a high emissivity coating on basic based refractories for high temperature application.

Conclusions

Mixtures of CeO_2 and $AlH_6O_{12}P_3$ heated with a rate of 1°C/min for 3h at 1300°C were examined as a potential coating for basic refractory bricks for application in cement kiln linings. Rheology studies show a shear thinning effect which is beneficial for the spraying process and the coating adhesion after spraying. XRD of the coating after heat treatment shows that $CePO_4$ formed more easily as CeO_2:$AlH_6O_{12}P_3$ ratio decreases. SEM revealed that the coating heat treated to 1300°C contained pores, $CePO_4$ nucleated from CeO_2 reacting with $AlH_6O_{12}P_3$, and melt like phase. TEM analysis confirmed that the nucleated particles are $CePO_4$ and the melt like phase is Mg-P-O glass. Coated brick emissivity after heating to 1300°C shows a significant improvement of 120% compared to un-coated brick. To reach the ultimate goal of the coating to act efficiently in the cement rotary kiln, abrasion, thermal shock and corrosion resistance should be studied further.

Acknowledgement

JJ was supported by SCG Cement-Building Material Co., Ltd, Bangkok, Thailand.

References

1. Madlool N, Saidur R, Rahim N, Kamalisarvestani M. An overview of energy savings measures for cement industries. Renewable and Sustainable Energy Reviews. 2013;19:18-29.
2. Engin T, Ari V. Energy auditing and recovery for dry type cement rotary kiln systems—A case study. Energy conversion and management. 2005;46(4):551-62.
3. Cheng J-JA, Martinez WA, Hale AP. Lightweight tundish refractory composition. United States Patent Office, 3150989; 1991.
4. Abyzov VA. Lightweight refractory concrete based on aluminum-magnesium-phosphate binder. Procedia Engineering. 2016;150:1440-5.

5. Macey CL, Knauss RJ. Low thermal conductivity magnesite-spinel brick and method. United States Patent, 4833109; 1989.

6. Modest MF. Radiative heat transfer: Academic press; 2013.

7. Huang J, Fan C, Song G, Li Y, He X, Zhang X, et al. Enhanced infrared emissivity of CeO_2 coatings by La doping. Applied Surface Science. 2013;280:605-9.

8. Huang J, Li Y, Song G, Zhang X, Sun Y, He X, et al. Highly enhanced infrared spectral emissivity of porous CeO_2 coating. Materials Letters. 2012;85:57-60.

9. Huang J, Song G, Lv H, Li Y, Sun Y, He X, et al. Microstructure and thermal cycling behavior of CeO_2 coatings deposited by the electron beam physical vapor technique. Thin Solid Films. 2013;544:270-5.

10. Holcombe Jr CE, Chapman LR. High emissivity coating. United States Patents, 5668072; 1997.

11. Tan W, Adducci M, Petorak C, Thompson B, Brenner AE, Trice RW. Effect of rare-earth dopant (Sm) concentration on total hemispherical emissivity and ablation resistance of ZrB_2/SiC coatings. Journal of the European Ceramic Society. 2016;36(16):3833-41.

12. Vippola M, Keränen J, Zou X, Hovmöller S, Lepistö T, Mäntylä T. Structural characterization of aluminum phosphate binder. Journal of the American Ceramic Society. 2000;83(7):1834-6.

13. Formanek B, Szymański K, Szczucka-Lasota B, Włodarczyk A. New generation of protective coatings intended for the power industry. Journal of Materials Processing Technology. 2005;164:850-5.

14. De Sousa Meneses D, Melin P, del Campo L, Cosson L, Echegut P. Apparatus for measuring the emittance of materials from far infrared to visible wavelengths in extreme conditions of temperature. Infrared Physics & Technology. 2015;69:96-101.

15. Juthapakdeeprasert J, Lerdprom W, De Sousa Meneses D, Jayaseelan DD, Lee WE, editors. CeO_2 and $CePO_4$ – containing high emissvity coating for basic refractory bricks. 61th International Colloquium on Refractories; 2018; Aachen, Germany.

16. Tsuhako M, Ikeuchi S, Matsuo T, Motooka I, Kobayashi M. Conditions of the formation of rare earth phosphates and the colors of their powders. Bulletin of the Chemical Society of Japan. 1979;52(4):1034-40.

17. Li Y, Chen L, Hong L, Ran K, Zhan Y, Chen Q. Fabrication of porous silicon carbide ceramics at low temperature using aluminum dihydrogen phosphate as binder. Journal of Alloys and Compounds. 2019;785:838-45.

18. Maslakov KI, Teterin YA, Ryzhkov MV, Popel AJ, Teterin AY, Ivanov KE, et al. The electronic structure and the nature of the chemical bond in CeO_2 Physical Chemistry Chemical Physics. 2018;20(23):16167-75.

19. Adelstein N, Mun BS, Ray HL, Ross Jr PN, Neaton JB, De Jonghe LC. Structure and electronic properties of cerium orthophosphate: Theory and experiment. Physical Review B. 2011;83(20):205104.
20. Brun J, Del Campo L, De Sousa Meneses D, Echegut P. Infrared optical properties of α-alumina with the approach to melting: γ-like tetrahedral structure and small polaron conduction. Journal of Applied Physics. 2013;114(22):223501.
21. Rousseau B, Brun J, Meneses DDS, Echegut P. Temperature measurement: Christiansen wavelength and blackbody reference. International Journal of Thermophysics. 2005;26(4):1277-86.

Captions

Figure 1. Viscosity of CeO_2 mixed with $AlH_6O_{12}P_3$ at different volume ratios.

Figure 2. Schematic of spraying process.

Figure 3. XRD of coatings heat treated at 1300°C, 3h. a) is of all three coatings for 15-65° 2theta, b) is a magnified image of a) for15-25° 2theta. The coating contained different ratios of the composition of CeO_2: $AlH_6O_{12}P_3$ of 1:3, 1:5 and 1:12 presented in green, red and blue, respectively. Circles (●) are CeO_2 and diamonds (■) are $CePO_4$.

Figure 4. SEM image of CBR 1:5 vol. CeO_2:$AlH_6O_{12}P_3$ cross section heat treated for 3h at 1300°C. a) overview image of the substrate and the coating. b) magnified image from boxed section shown in a) revealing pores, large grains (~10μm), small grains (~2μm) and a likely melt-formed phase. c) magnified image from boxed section shown in b) revealing large (CeO_2) and small grains ($CePO_4$).

Figure 5. SEM and EDX image of CBR 1:5 vol. CeO_2:$AlH_6O_{12}P_3$ cross section heat treated for 3h at 1300°C

Figure 6. Schematic of cross section 1:5 ratio of CeO_2:$AlH_6O_{12}P_3$ coating on substrate developing as temperature increase. a) At room temperature, CeO_2 particles settle in the $AlH_6O_{12}P_3$ binder. b) At 900°C, dehydrogenation of $AlH_6O_{12}P_3$ occurs generating pores and $CePO_4$ starts forming. c) At 1300°C, $CePO_4$ continues forming and the remaining CeO_2 sinters.

Figure 7. STEM-EDX microstructure of the coating 1-5 a) STEM bright field image of particles (P) and matrix (M) area. b) EDX map of magnified (box) section shown in a). c) TEM diffraction pattern of $CePO_4$ particles. d) Electron diffraction pattern of matrix indicating its glassy nature.

Figure 8. (a) Emissivity of BR and CBR at 1100°C and 1300°C. The x-axis presents wavenumber (cm^{-1}) ranging from 700-12000 cm^{-1} and the y-axis of the graph presents emissivity ranging 0-1. The red dash line, red solid line, black dash line, and black solid line represents BR emissivity at 1100°C, BR emissivity at 1300°C, CBR emissivity at 1100°C and CBR emissivity at 1300°C respectively. (b) magnified image from section shown in a) revealing Christiansen point, stretching of PO_4 bond and effect from the CO_2 laser.

Table 1. Power and temperatures achieve for BR and CBR

Table 1 Power and temperatures achieve for BR and CBR

Power (Watts)	BR temperature (^{o}C)	CBR temperature (^{o}C)
18	505 ±20	540 ±20
36	921 ±20	919 ±20
54	1125 ±20	1077 ±20
71	1319 ±20	1194 ±20
100	1550 ±20	1328 ±20

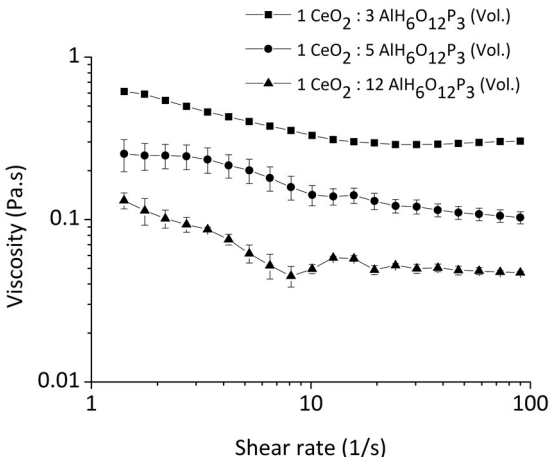

ijac_13416_f1.jpg

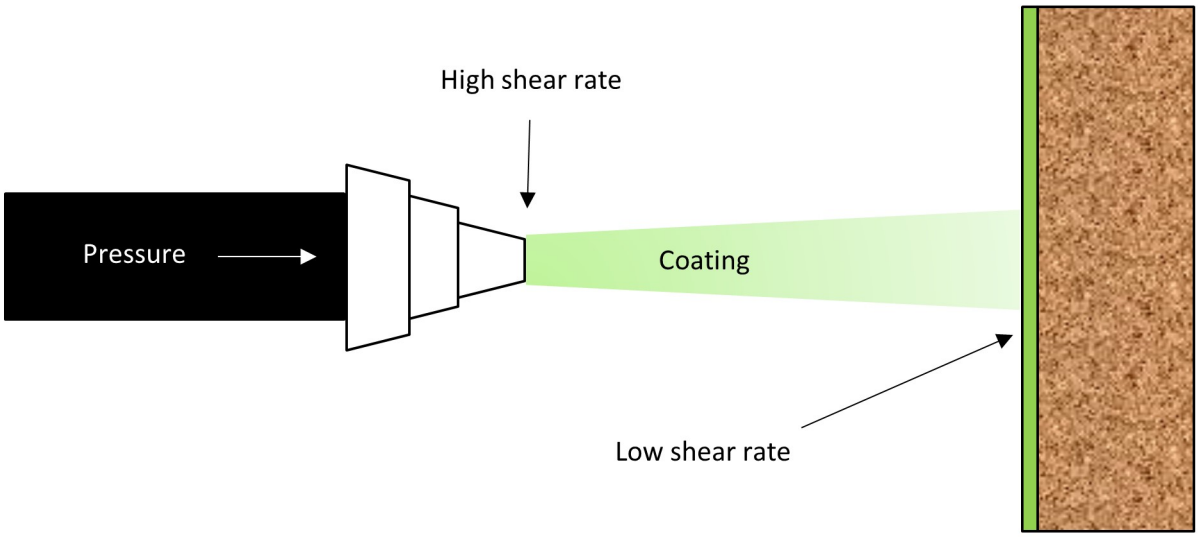

ijac_13416_f2.jpg

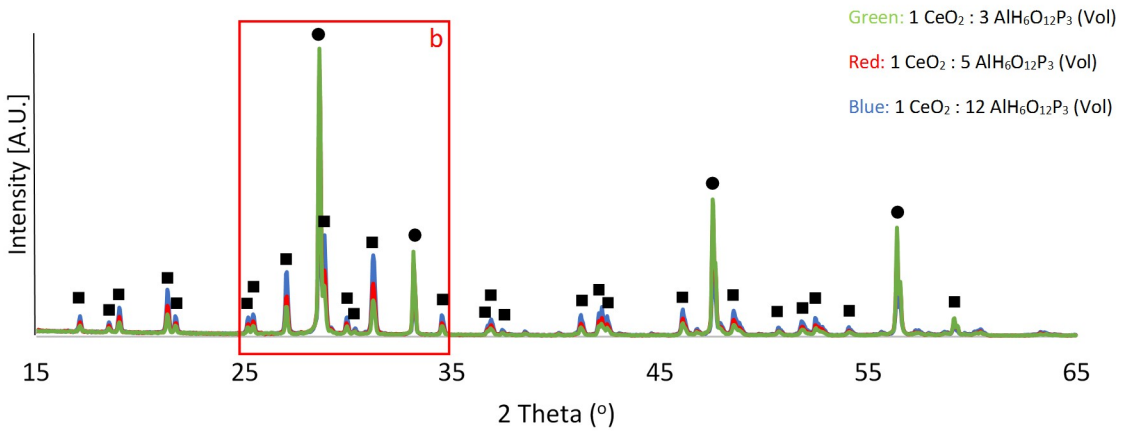

(a)

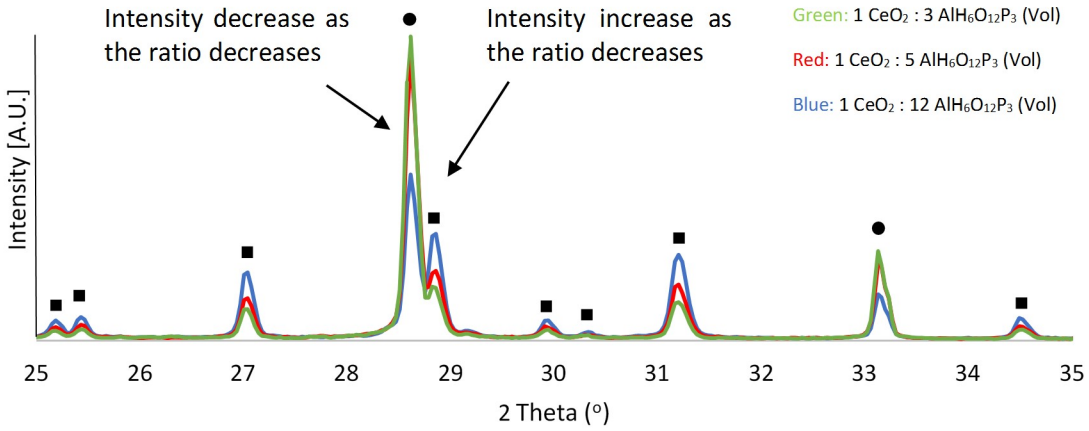

(b)

ijac_13416_f3.jpg

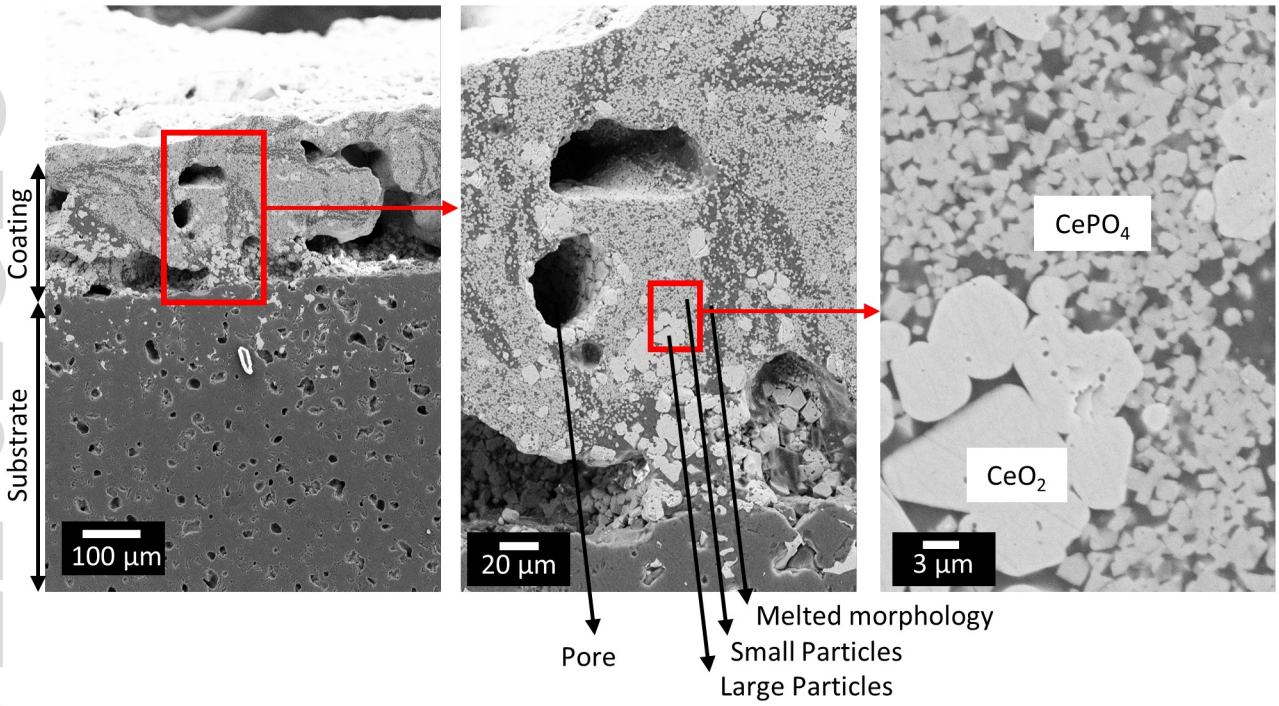

ijac_13416_f4.jpg

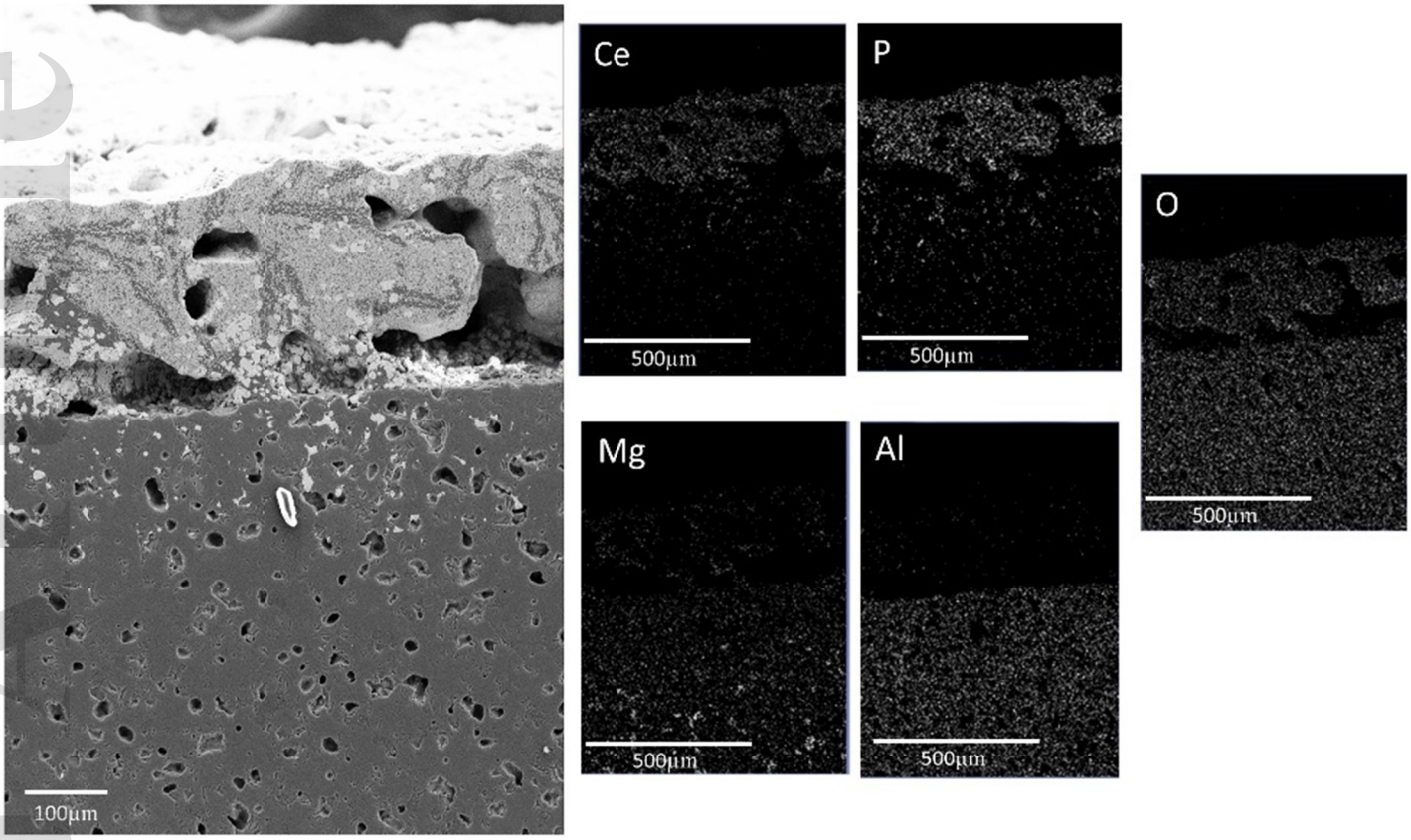

ijac_13416_f5.jpg

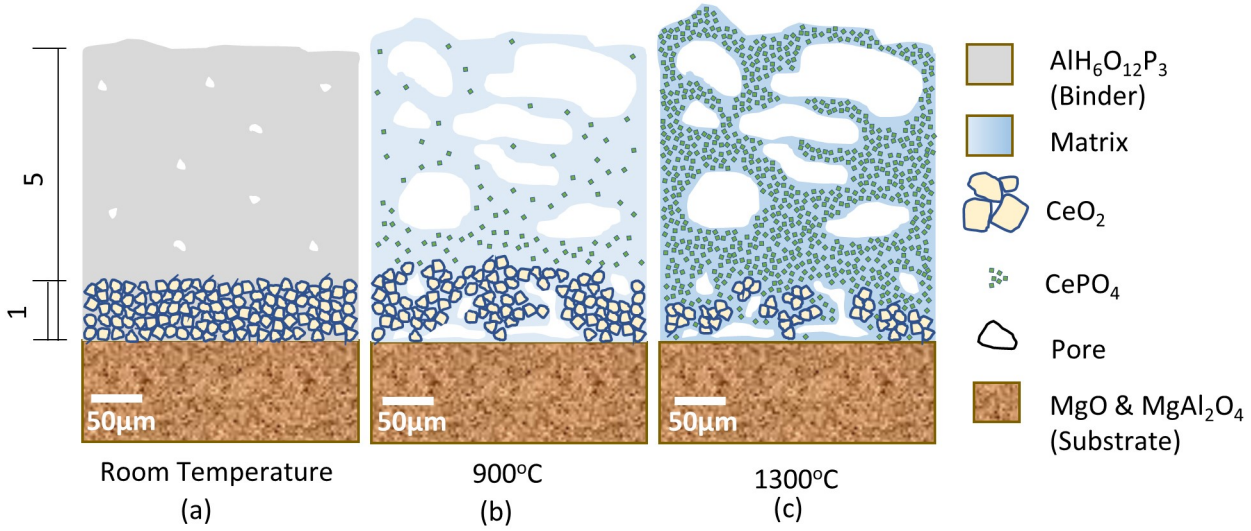

ijac_13416_f6.jpg

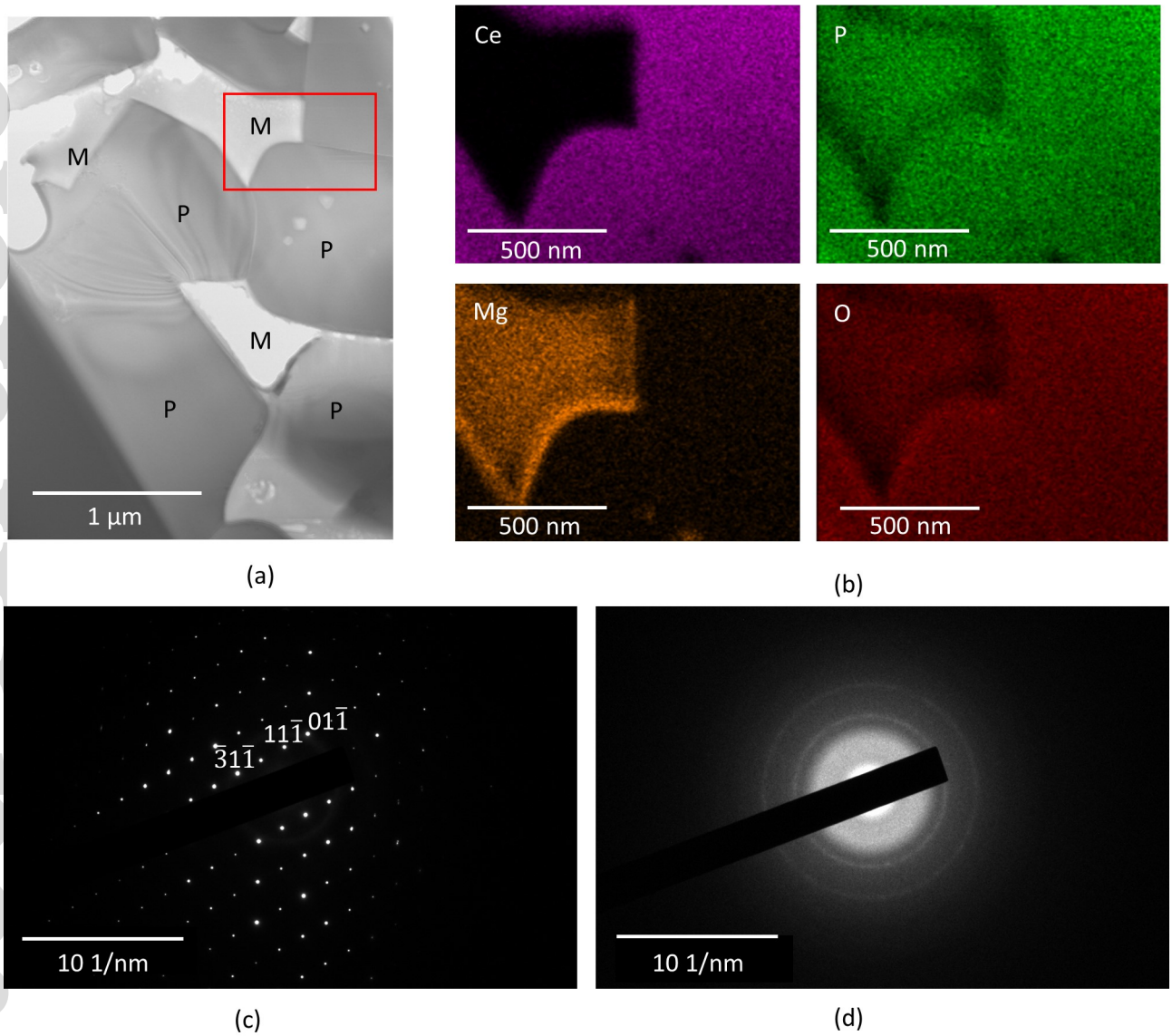

ijac_13416_f7.jpg

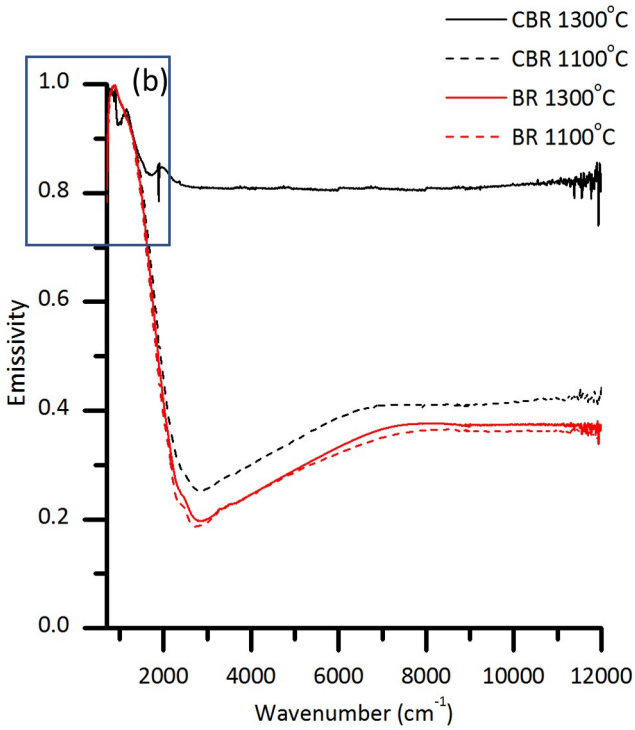

(a)

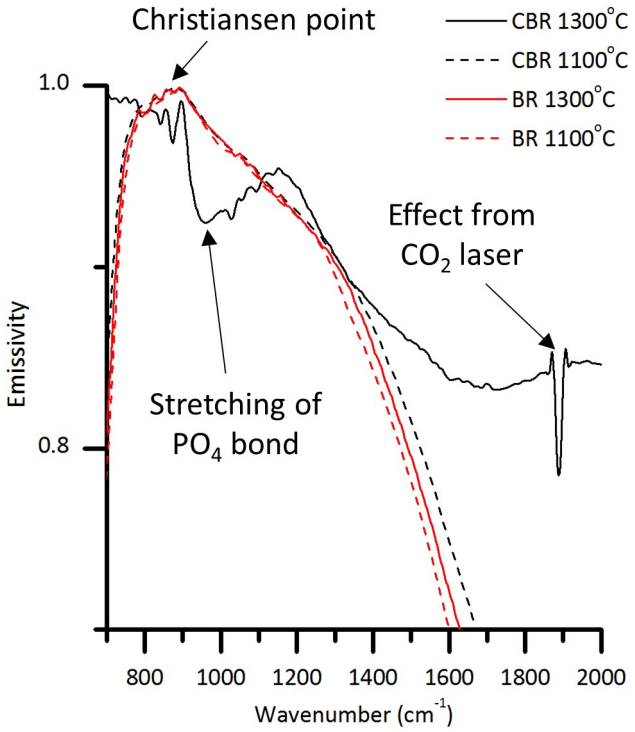

(b)

ijac_13416_f8.jpg